Supplementary Information

Effective Interfacial Energy Band Engineering Strategy toward High-performance Triboelectric Nanogenerator

Xinkai Xie[1, 2, 3, #], Yuxiao Fang[2, 3, 4, #], Cheng Lu[1], Yi Tao[1], Li Yin[2, 3], Yibo Zhang[2], Zixin Wang[2], Shiyan Wang[2], Jianwen Zhao[4], Xin Tu[3], Xuhui Sun[1], Eng Gee Lim[2], Chun Zhao[2, *], Yina Liu[2, *], Zhen Wen[1, *]

[1] Institute of Functional Nano and Soft Materials (FUNSOM), Jiangsu Key Laboratory for Carbon-Based Functional Materials and Devices, Soochow University, Suzhou 215123, China.

[2] School of Advanced Technology, School of Science, Xi'an Jiaotong-Liverpool University, Suzhou 215123, China.

[3] Department of Electrical and Electronic Engineering, University of Liverpool, Liverpool L693GJ, United Kingdom.

[4] Printable Electronics Research Centre, Suzhou Institute of Nano-Tech and Nano-Bionics, Chinese Academy of Sciences, Suzhou 215123, China.

[#] X. Xie, and Y. Fang contributed equally to this work.

*Corresponding Author: Chun.Zhao@xjtlu.edu.cn (C. Zhao); Yina.Liu@xjtlu.edu.cn (Y. Liu); wenzhen2011@suda.edu.cn (Z. Wen).

Supplementary Note S1

Energy band calculation formula

$$W_F = 21.22\ eV - E_{cut-off}$$

$$E_F = 0 - W_F$$

$$E_V = E_F - E_{onset}$$

$$E_C = E_V + E_g$$

Supplementary Note S2

To calculate the relative permittivity of ZrO_x, $La_{0.1}Zr_{0.9}O_x$, and $La_{0.2}Zr_{0.8}O_x$ HPEBL, the equation can be expressed by:

$$\varepsilon_r = \frac{C_{area} \cdot d}{\varepsilon_0}$$

Where the measured average area capacitance C_{area} of ZrO_x, $La_{0.1}Zr_{0.9}O_x$, and $La_{0.2}Zr_{0.8}O_x$ HPEBL shown in Figure 4c are 488.4 nF cm^{-2}, 355.1 nF cm^{-2}, and 333.5 nF cm^{-2}. The thicknesses of the ZrO_x, $La_{0.1}Zr_{0.9}O_x$, and $La_{0.2}Zr_{0.8}O_x$ HPEBL are 35nm, 55 nm, and 60 nm. The diameter of the MIM unit shown in the red frame of Figure 4a is 0.3 mm, thus the area size is $2.83 \times 10^{-7}\ m^2$.

Therefore, the calculated results of relative permittivity of ZrO_x, $La_{0.1}Zr_{0.9}O_x$, and $La_{0.2}Zr_{0.8}O_x$ HPEBL can be listed in the following table:

	ZrO_x	$La_{0.1}Zr_{0.9}O_x$	$La_{0.2}Zr_{0.8}O_x$
ε_r	19.3	22	22.6

Supplementary Note S3

We constructed the intermediate layer based TENG shown in following figure to derive the relationship between maximum surface charge density (σ_m) and the thickness of the intermediate layer (d_2). According to Gauss's law:

$$E_1 = \frac{-\sigma_x}{\varepsilon_0 \varepsilon_{r1}} \tag{1}$$

$$E_2 = \frac{-\sigma_x}{\varepsilon_0 \varepsilon_{r2}} \tag{2}$$

$$E_{air} = \frac{-\sigma_x + \sigma_0}{\varepsilon_0} \tag{3}$$

And the total potential difference could be expressed as:

$$\Delta V_E = E_{air} x + E_1 d_1 + E_2 d_2 = -\frac{\sigma_x}{\varepsilon_0}\left(\frac{d_1}{\varepsilon_{r1}} + \frac{d_2}{\varepsilon_{r2}} + x\right) + \frac{\sigma_0 x}{\varepsilon_0} \tag{4}$$

Let $d_0 = \frac{d_1}{\varepsilon_{r1}} + \frac{d_2}{\varepsilon_{r2}}$

At short-circuit, let $\Delta V_E = 0$

Then we obtain $\sigma_x = \frac{\sigma_0 x}{\frac{d1}{\varepsilon_{r1}} + \frac{d_2}{\varepsilon_{r2}} + x} = \frac{\sigma_0 x}{d_0 + x}$

According to the capacitor model:

$$V_{gap} = \frac{\sigma_0 d_0 x}{\varepsilon_0 (d_0 + x)} \tag{5}$$

Considering the limitation of Paschen's law:

$$V = \frac{BPx}{ln(Px) + C} \tag{6}$$

And we let $V_{gap} = \mathrm{V}$ to get the maximum surface charge density σ_m:

$$\sigma_m = \left(\frac{BP\varepsilon_0(d_0+x)}{(ln(Px)+C)d_0}\right)_{min} = \left(\frac{BP\varepsilon_0\left(1+\frac{x}{d_0}\right)}{(ln(Px)+C)}\right)_{min} \tag{7}$$

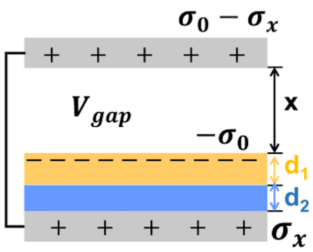

Charge distribution model of intermediate layer based TENG

According to the above expression of σ_m, the maximum surface charge density increases as the effective thickness decreases. In this case, only the influence of thickness variable is considered, and the impact of possible polarization field or polarizability is neglected.

Supplementary Note S4

Calculation on output power and energy conversion efficiency

The following table shows parameters of the $La_{0.1}Zr_{0.9}O_x$ HPEBL based TENG:

Parameter	Value
Mass of the device without Al: m_d	0.3936 g
Mass of the whole device: m_{TENG}	0.4112 g
Volume of the whole device: V_{TENG}	0.16 cm^3
Maximum separation distance: x_{max}	4 mm
Operation frequency: f	2 Hz
Thickness of PDMS: d_1	10 μm
Thickness of intermediate layer $La_{0.1}Zr_{0.9}O_x$: d_2	0.05 μm
Relative permittivity of PDMS: ε_{r1}	2.64
Relative permittivity of $La_{0.1}Zr_{0.9}O_x$: ε_{r2}	22
Effective thickness of the dielectric layer: $d_0 = d_1/\varepsilon_{r1} + d_2/\varepsilon_{r2}$	3.79 μm
Surface charge: Q	97.3 nC
Contact surface area: S	4 cm^2
Maximized output energy per cycle: $E_{per\ cycle}$	12.2 μJ

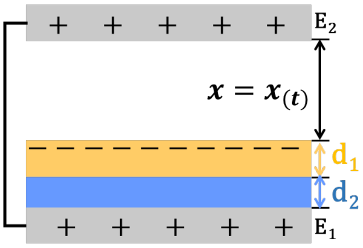

Model of the $La_{0.1}Zr_{0.9}O_x$ HPEBL based TENG

$$P_{mass} = \frac{E_{per\ cycle}}{t_{per\ cycle} \cdot m} = \frac{12.2 \mu J}{0.5\ s \times 0.4112\ g} = 59.34\ \mu W/g$$

$$P_{volume} = \frac{E_{per\ cycle}}{t_{per\ cycle} \cdot V} = \frac{12.2 \mu J}{0.5\ s \times 0.16\ cm^3} = 152.5\ \mu W/cm^3$$

$$Q_{E_1} = Q_{SC(t)} = \frac{S\sigma x(t)}{d_0 + x(t)} = \frac{Qx(t)}{d_0 + x(t)}$$

$$Q_{dielectric} = -Q$$

$$Q_{fixed} = Q_{E_1} + Q_{dielectric} = \frac{Qx(t)}{d_0 + x(t)} - Q = -\frac{Qd_0}{d_0 + x(t)}$$

From Gauss theorem: $E_{fixed} = \frac{|Q_{fixed}|}{2S\varepsilon_0} = \frac{Qd_0}{2S\varepsilon_0[d_0+x(t)]}$

$$Q_{E_2} = -Q_{fixed} = \frac{Qd_0}{d_0 + x(t)}$$

$$W_{electrostatic\,force} = F \cdot x(t) = E_{fixed} \cdot Q_{E_2} \cdot x(t)$$

$$= \frac{Qd_0}{2S\varepsilon_0[d_0 + x(t)]} \cdot \frac{Qd_0}{d_0 + x(t)} \cdot x(t) = \frac{(Qd_0)^2 x(t)}{2S\varepsilon_0[d_0 + x(t)]^2}$$

Energy due to electrostatic force of half cycle:

$$W_{electrostatic\,force} = \int_0^{x_{max}} \frac{(Qd_0)^2 x(t)}{2S\varepsilon_0[d_0 + x(t)]^2} d_x$$

Gravimetric Power Density	Volumetric Power Density	Energy Conversion Efficiency
59.34 $\mu W/g$	152.5 $\mu W/cm^3$	39.2%

Therefore, the total input energy of half cycle:

$$E_{input} = mgx_{max} + W_{electrostatic\,force}$$

$$= 1.542912 \times 10^{-5}\,J + 1.145454 \times 10^{-10}\,J = 15.5436654\,\mu J$$

$$E_{output} = E_{per\,cycle}/2 = 6.1\,\mu J$$

$$\eta = E_{output}/E_{input} \times 100\% = 6.1\,\mu J/15.5436654\,\mu J \times 100\% = 39.2\%$$

The summarized gravimetric power density, volumetric power density and energy conversion efficiency of the $La_{0.1}Zr_{0.9}O_x$ HPEBL based TENG are listed in the following table.

Supplementary Note S5

The interfacial electric field applied between to the HPEBL can be calculated with the following equation:

$$E = \frac{Q}{S\varepsilon_0\varepsilon_r}$$

Where the maximized charge density could be smaller than the transfer charge density Q/S=243.3 μC m^{-2}. Therefore, for intermediate layers with different relative permittivity, the calculated maximum interfacial electric field can be presented as 0.0142 MV/cm, 0.0125 MV/cm and 0.0122 MV/cm with ZrO_x, $La_{0.1}Zr_{0.9}O_x$, and $La_{0.2}Zr_{0.8}O_x$ layer. Combined with the measured leakage current shown in Figure 4d, the leakage current outputs are 5.68×10^{-5} A/m^2, 3.07×10^{-5} A/m^2 and 1.02×10^{-4} A/m^2 respectively. The $La_{0.1}Zr_{0.9}O_x$ film possess the best anti-leakage performance.

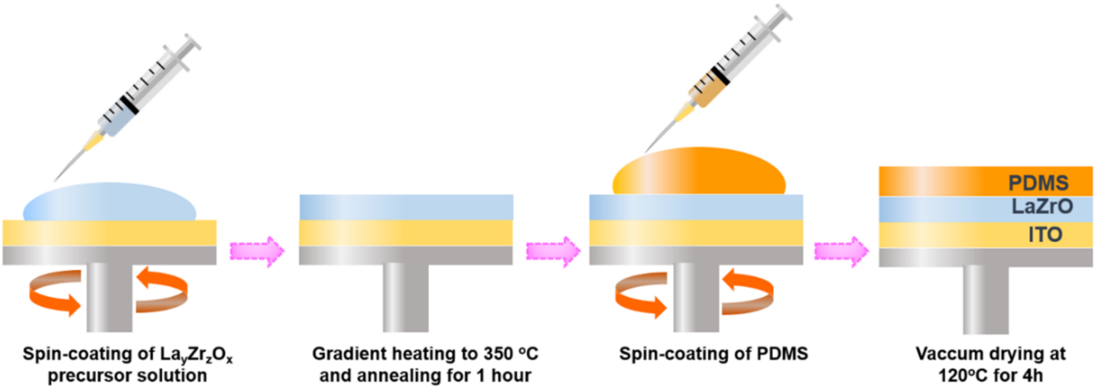

Fig. S1 Fabrication process of the LaZrO HPEBL based TENG.

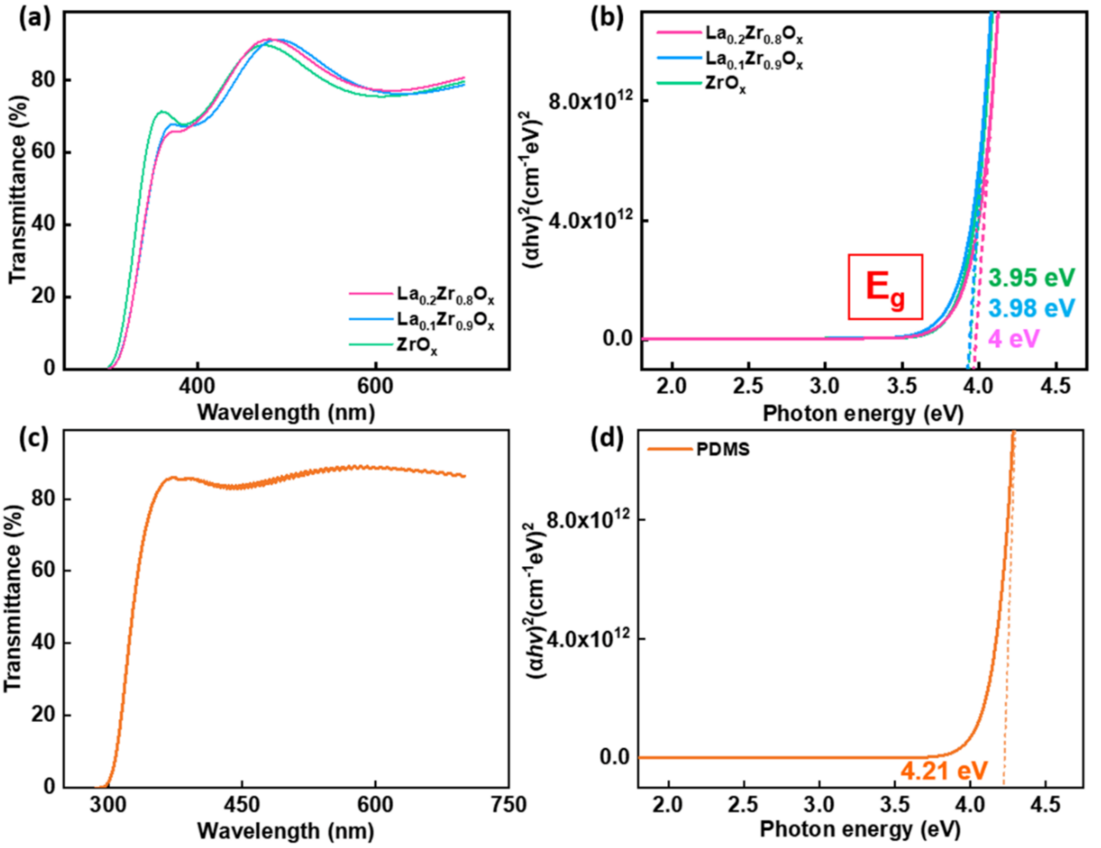

Fig. S2 (a) Transmittance spectra and (b) Evaluation of the $(ahv)^2$ versus hv curves of various LaZrO films with a role of La content varying from 0 to 20%. (c) Transmittance spectra and (d) Evaluation of the $(ahv)^2$ versus hv curves of PDMS.

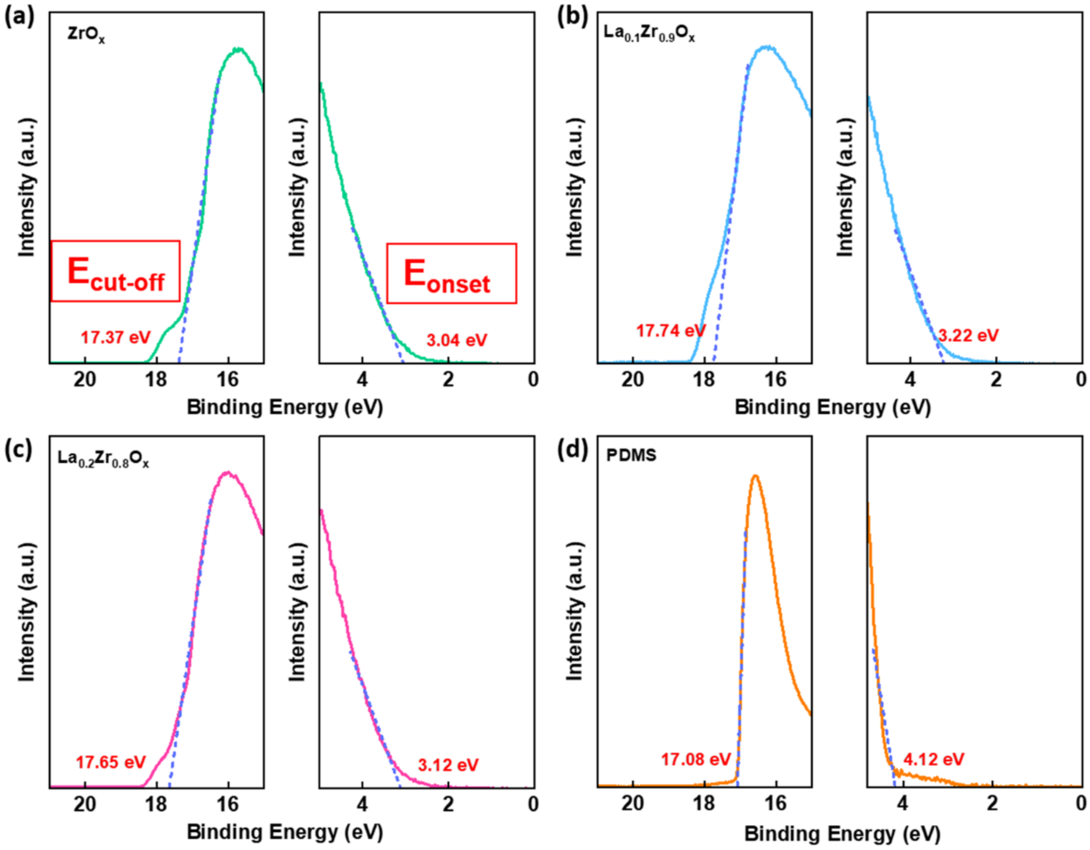

Fig. S3 Ultraviolet Photoelectron Spectrometer (UPS) pattern of (a) ZrO_x, (b) $La_{0.1}Zr_{0.9}O_x$, (c) $La_{0.2}Zr_{0.8}O_x$, and (d) PDMS respectively.

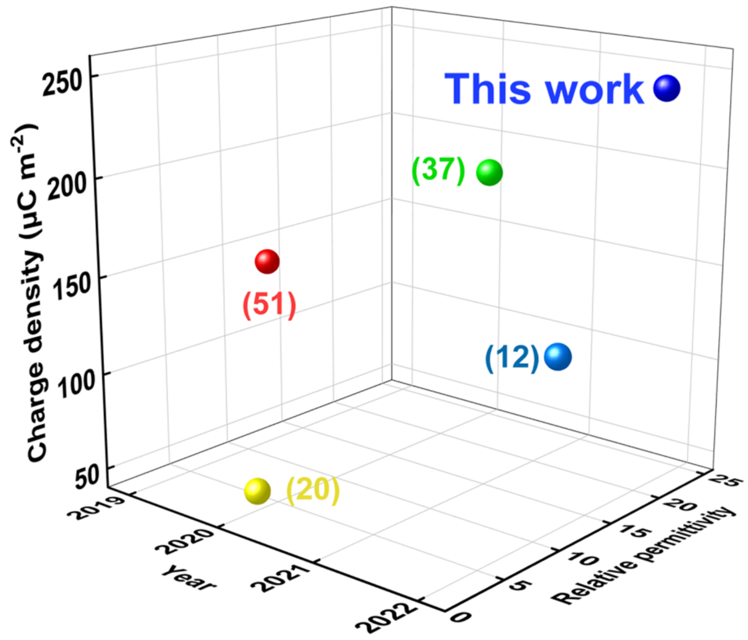

Fig. S4 Comparison to recent works about relative permittivity and transferred charge density.

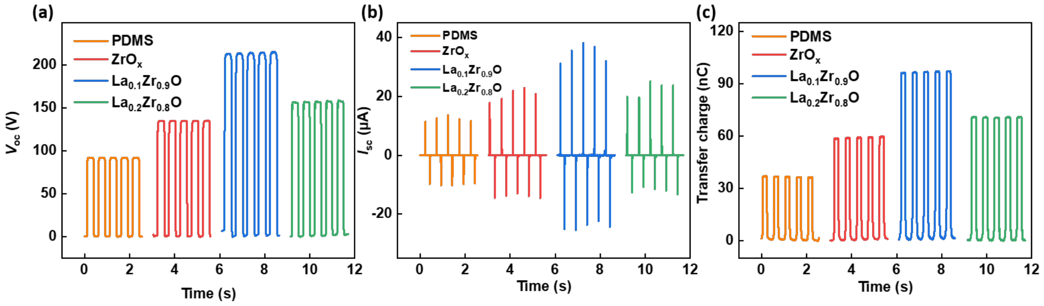

Fig. S5 (a) Open-circuit voltage, (b) Short-circuit current and (c) Transferred charge density of different TENG devices without LaZrO, with ZrO$_x$, La$_{0.1}$Zr$_{0.9}$O$_x$, and La$_{0.2}$Zr$_{0.8}$O$_x$, respectively.

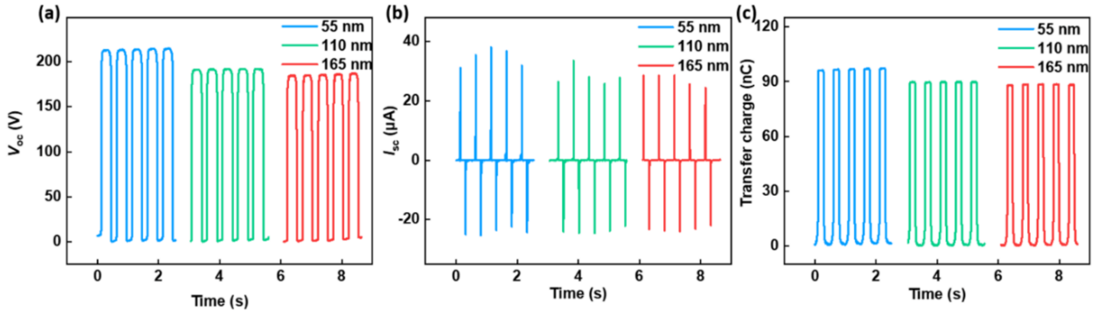

Fig. S6 (a) Open-circuit voltage, (b) Short-circuit current and (c) Transferred charge density of different TENG devices with different thicknesses of $La_{0.1}Zr_{0.9}O_x$.

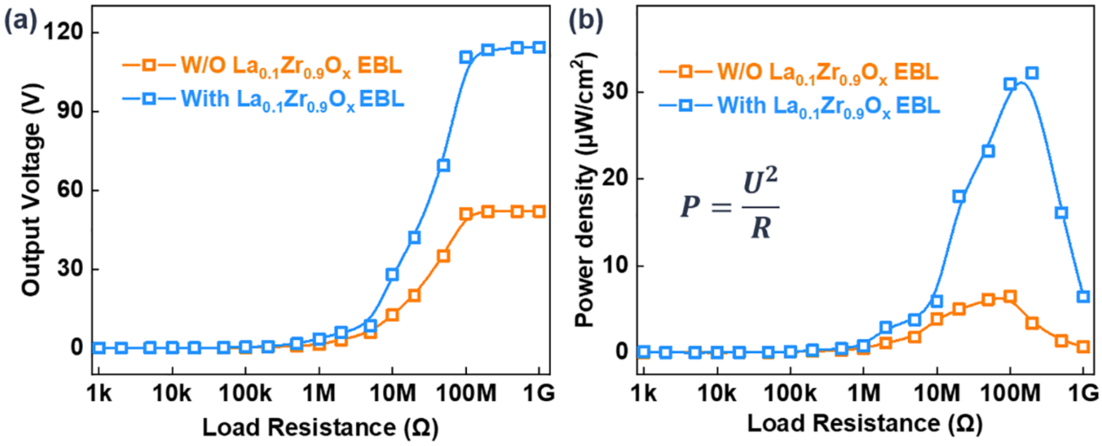

Fig. S7 Variation of voltage and peak power density as a function of load resistance.

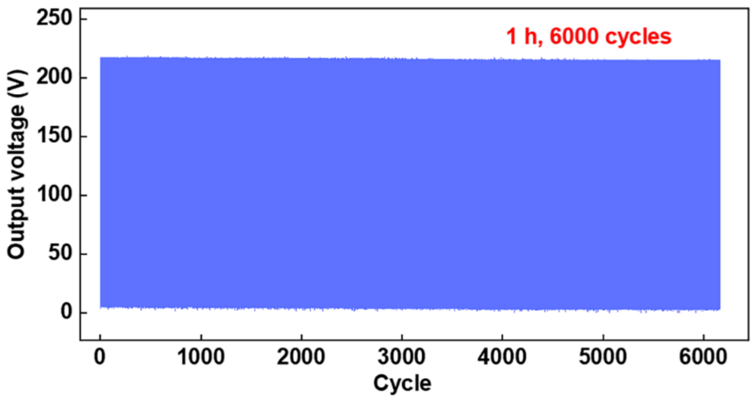

Fig. S8 Stability of $La_{0.1}Zr_{0.9}O_x$ HPEBL based TENG.

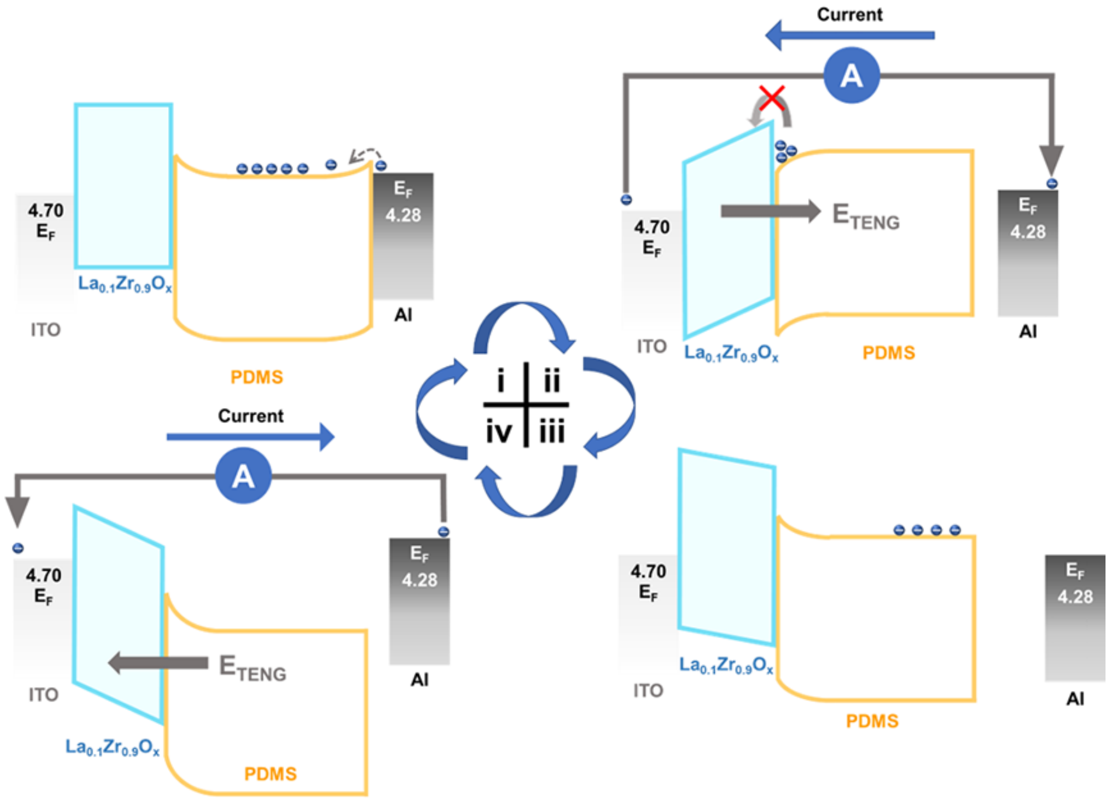

Fig. S9 The band alignment of $La_{0.1}Zr_{0.9}O_x$ based TENG during different states of a single contact separation cycle.

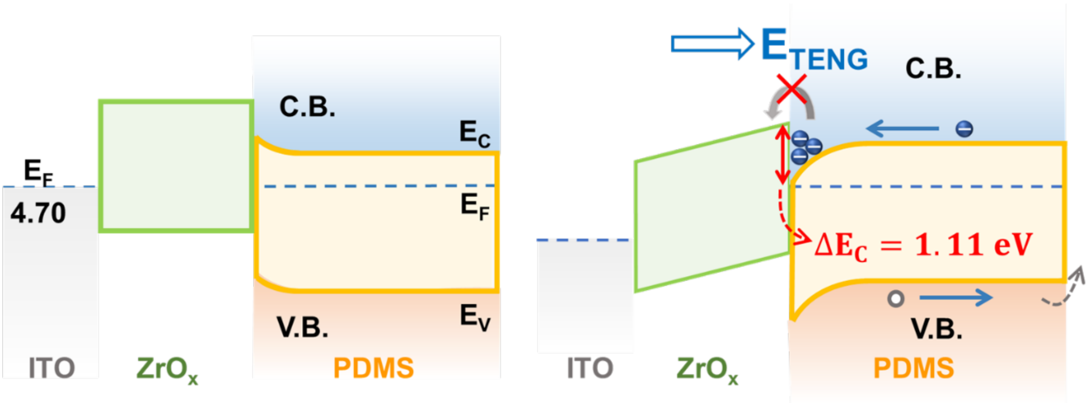

Fig. S10 Energy band diagram of ZrO_x based TENG before and (h) after triboelectrification.

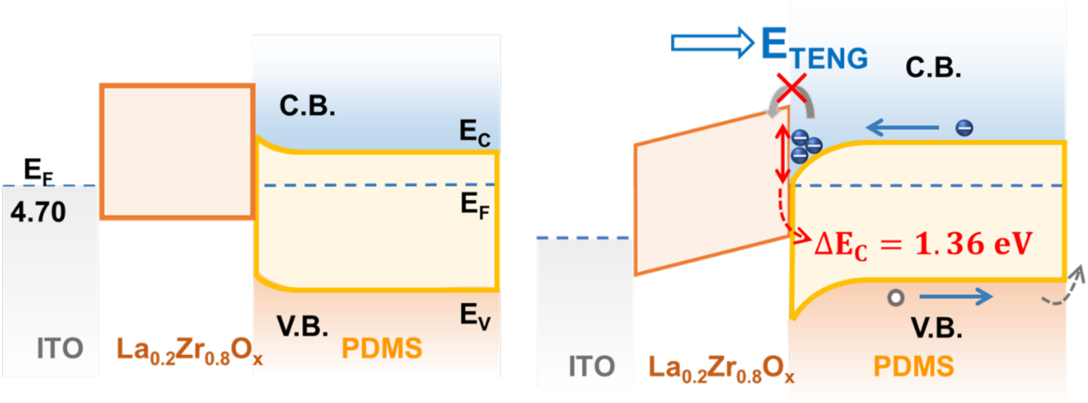

Fig. S11 Energy band diagram of $La_{0.2}Zr_{0.8}O_x$ based TENG before and (h) after triboelectrification.

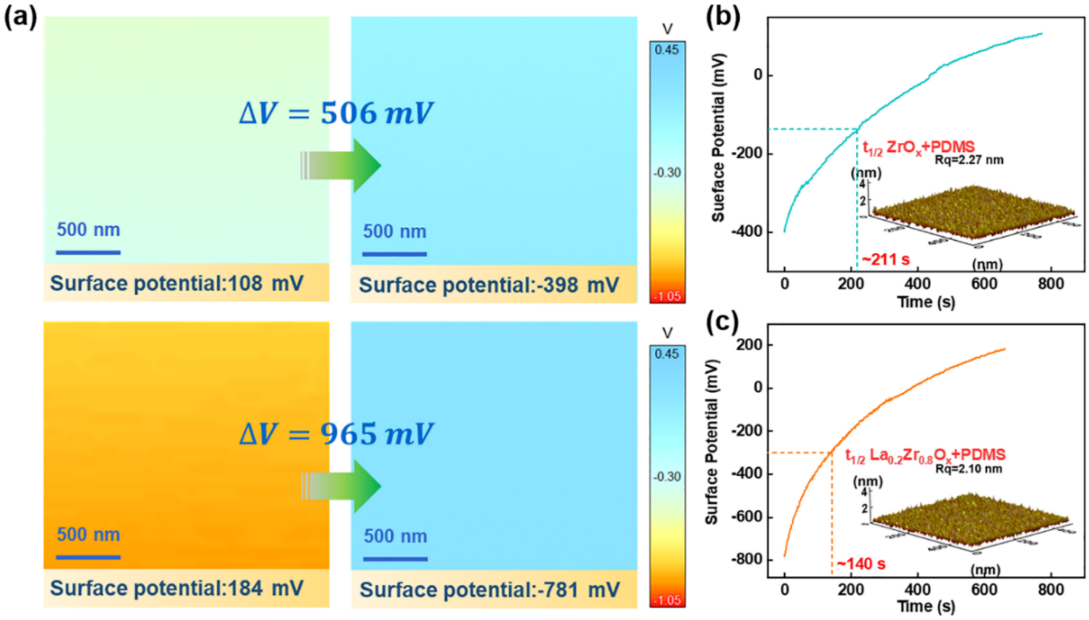

Fig. S12 Contact potential difference and surface charge decay pattern of ZrO_x H-TENG and $La_{0.2}Zr_{0.8}O_x$ H-TENG.

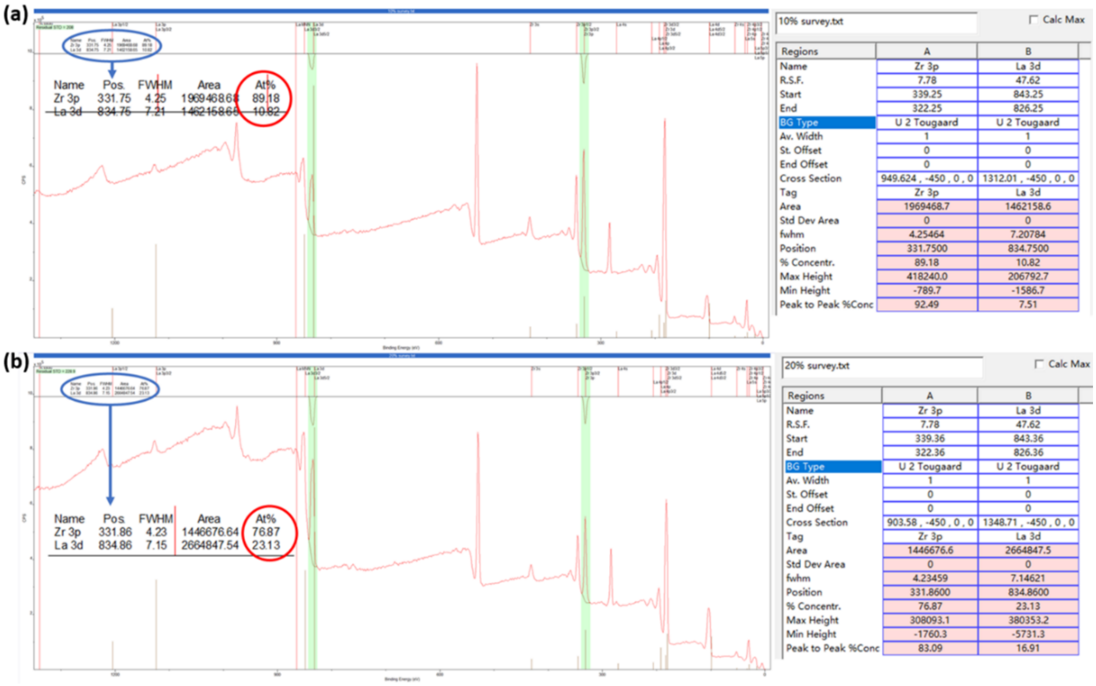

Name	Pos.	FWHM	Area	At%
Zr 3p	331.75	4.25	1969468.68	89.18
La 3d	834.75	7.21	1462158.65	10.82

10% survey.txt

☐ Calc Max

Regions	A	B
Name	Zr 3p	La 3d
R.S.F.	7.78	47.62
Start	339.25	843.25
End	322.25	826.25
BG Type	U 2 Tougaard	U 2 Tougaard
Av. Width	1	1
St. Offset	0	0
End Offset	0	0
Cross Section	949.624 , -450 , 0 , 0	1312.01 , -450 , 0 , 0
Tag	Zr 3p	La 3d
Area	1969468.7	1462158.6
Std Dev Area	0	0
fwhm	4.25464	7.20784
Position	331.7500	834.7500
% Concentr.	89.18	10.82
Max Height	418240.0	206792.7
Min Height	-789.7	-1586.7
Peak to Peak %Conc	92.49	7.51

Name	Pos.	FWHM	Area	At%
Zr 3p	331.86	4.23	1446676.64	76.87
La 3d	834.86	7.15	2664847.54	23.13

20% survey.txt

☐ Calc Max

Regions	A	B
Name	Zr 3p	La 3d
R.S.F.	7.78	47.62
Start	339.36	843.36
End	322.36	826.36
BG Type	U 2 Tougaard	U 2 Tougaard
Av. Width	1	1
St. Offset	0	0
End Offset	0	0
Cross Section	903.58 , -450 , 0 , 0	1348.71 , -450 , 0 , 0
Tag	Zr 3p	La 3d
Area	1446676.6	2664847.5
Std Dev Area	0	0
fwhm	4.23459	7.14621
Position	331.8600	834.8600
% Concentr.	76.87	23.13
Max Height	308093.1	380353.2
Min Height	-1760.3	-5731.3
Peak to Peak %Conc	83.09	16.91

Fig. S13 CasaXPS software utilized to calculated the atomic ratio according to XPS survey spectra.

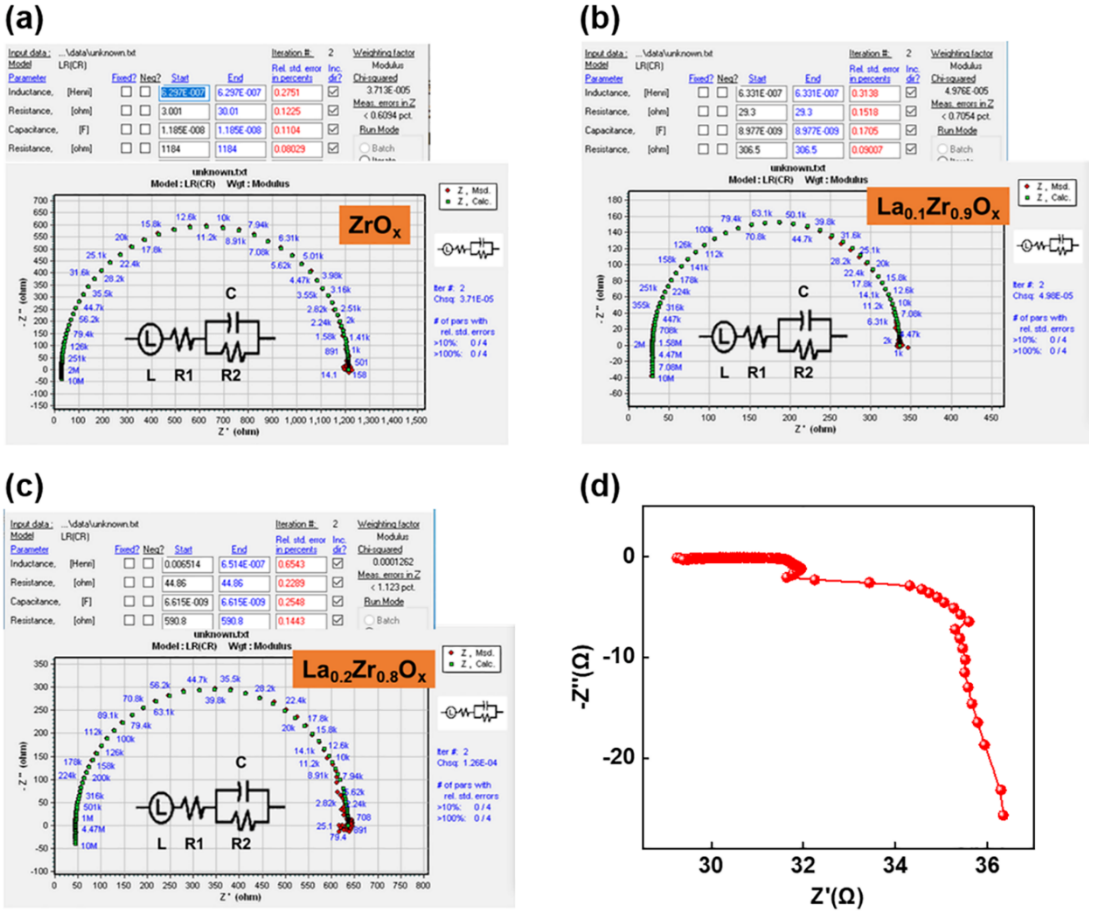

(a)

Input data : ...\data\unknown.txt

Model LR(CR)

Iteration #: 2

Parameter		Fixed?	Neg?	Start	End	Rel. std. error in percents	Inc. dir?
Inductance,	[Henri]	☐	☐	6.297E-007	6.297E-007	0.2751	☑
Resistance,	[ohm]	☐	☐	3.001	30.01	0.1225	☑
Capacitance,	[F]	☐	☐	1.185E-008	1.185E-008	0.1104	☑
Resistance,	[ohm]	☐	☐	1184	1184	0.08029	☑

Weighting factor: Modulus

Chi-squared: 3.713E-005

Meas. errors in Z: < 0.6094 pct.

Run Mode: ○ Batch

Iter #: 2

Chsq: 3.71E-05

# of pars with rel. std. errors >10%: 0 / 4 >100%: 0 / 4

(b)

Input data : ...\data\unknown.txt

Model LR(CR)

Iteration #: 2

Parameter		Fixed?	Neg?	Start	End	Rel. std. error in percents	Inc. dir?
Inductance,	[Henri]	☐	☐	6.331E-007	6.331E-007	0.3138	☑
Resistance,	[ohm]	☐	☐	29.3	29.3	0.1518	☑
Capacitance,	[F]	☐	☐	8.977E-009	8.977E-009	0.1705	☑
Resistance,	[ohm]	☐	☐	306.5	306.5	0.09007	☑

Weighting factor: Modulus

Chi-squared: 4.976E-005

Meas. errors in Z: < 0.7054 pct.

Run Mode: ○ Batch

Iter #: 2

Chsq: 4.98E-05

# of pars with rel. std. errors >10%: 0 / 4 >100%: 0 / 4

(c)

Input data : ...\data\unknown.txt

Model LR(CR)

Iteration #: 2

Parameter		Fixed?	Neg?	Start	End	Rel. std. error in percents	Inc. dir?
Inductance,	[Henri]	☐	☐	0.006514	6.514E-007	0.6543	☑
Resistance,	[ohm]	☐	☐	44.86	44.86	0.2289	☑
Capacitance,	[F]	☐	☐	6.615E-009	6.615E-009	0.2548	☑
Resistance,	[ohm]	☐	☐	590.8	590.8	0.1443	☑

Weighting factor: Modulus

Chi-squared: 0.0001262

Meas. errors in Z: < 1.123 pct.

Run Mode: ○ Batch

Iter #: 2

Chsq: 1.26E-04

# of pars with rel. std. errors >10%: 0 / 4 >100%: 0 / 4

Fig. S14 The EIS measurement results and simulated parameters of (a) ZrO_x, (b) $La_{0.1}Zr_{0.9}O_x$, (c) $La_{0.2}Zr_{0.8}O_x$ and (d) ITO thin films.

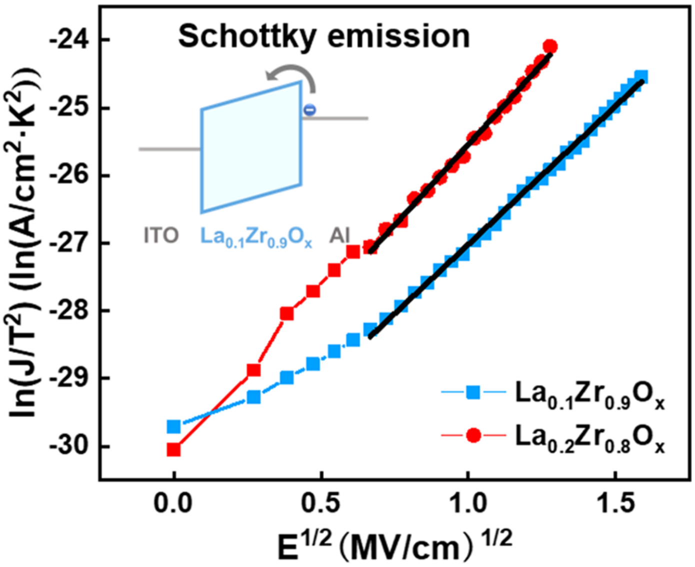

Fig. S15 Schottky emission plot of LaZrO films with La concentration varying from 10 to 20%.

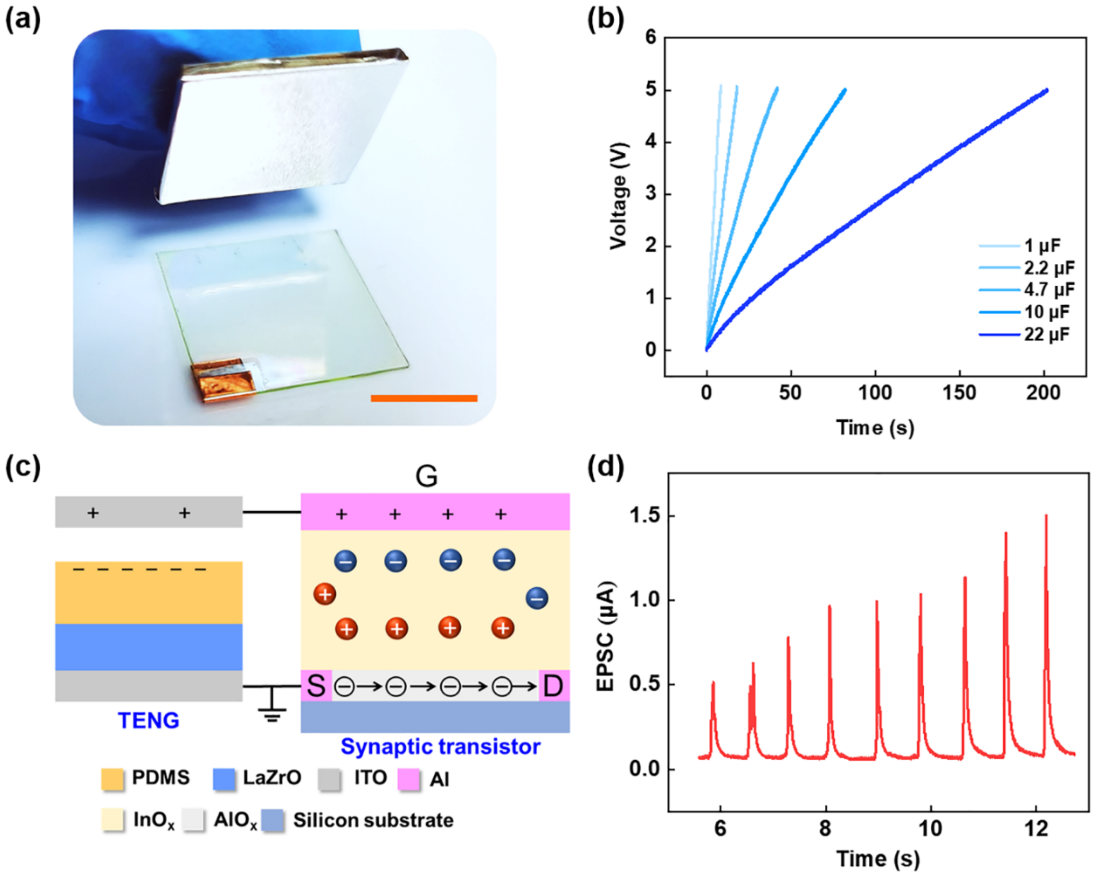

Fig. S16 Device of the $La_{0.1}Zr_{0.9}O_x$ based H-TENG and two practical applications. (a) Optical photograph of the $La_{0.1}Zr_{0.9}O_x$ based H-TENG, (b) application of charging different capacitors, (c) cross-section view and (d) application of contact electrification activated biological synaptic behavior.